AIAA 79-1133R

Nitramine Flame Chemistry and Deflagration Interpreted in Terms of a Flame Model

Moshe Ben-Reuven* and Leonard H. Caveny†
Princeton University, Princeton, N.J.

The diversity of chemical kinetic time scales associated with nitramine decomposition has led to incorporation of two simultaneous overall reactions in the vapor phase mode of deflagration. This allowed derivation of an asymptotic burning rate formula, showing variable pressure dependence. The comprehensive model considers a reacting melt layer, coupled to the gas field through conservation conditions satisfied by all chemical species and enthalpy, and is solved numerically. The structure of the deflagration wave near the propellant surface is obtained, along with the overall pressure dependence of the surface temperature and the flame speed eigenvalue, comparing RDX and HMX. A mechanism of coupling between secondary reactions and heat feedback to the surface is proposed, and a quantitative measure of the effect of condensed phase exothermicity on burning rate is demonstrated.

Nomenclature

A = pre-exponential factor, Arrhenius kinetics constant; 1/s for first order, m^3/mol-s for second order (Fig. 1)
a = proportionality constant, burning rate formula, Eq. (6)
B_p = reference pressure parameter, $F_1(\bar{T}_1)/F_2(\bar{T}_2)$, in burning rate formula, Eq. (6), MPa
C_p, C_c = specific heats for gas (isobaric) and condensed phase, respectively, J/kg-K
D = diffusion coefficient, gas mixture, m^2/s
E = activation energy, Arrhenius kinetics constant, kcal/mol (Fig. 1)
F_i = pressure-independent factor in mean reaction rate terms, $\bar{w}_1 = pF_1(\bar{T}_1)$, $\bar{w}_2 = p^2F_2(\bar{T}_2)$
g_c = dimensionless measure of condensed phase exothermicity effect upon burning rate
h_T = specific thermal enthalpy, defined by Eq. (10), J/kg
k_1, k_2 = reaction rate constant (Arrhenius form intended)
K_B = melt layer porosity coefficient, defined by Eq. (19)
m = mass burning rate, kg/m^2-s
n = burning rate pressure exponent in ap^n formula
p = pressure, MPa
Q = heat of reaction, J/mol
q_c = surface heat balance parameter (representing liquid side) defined in Eq. (16c)
R_u = universal gas constant, 1.987 cal/mol-K. In equation of state, SI units used
T = temperature, K
t_{c1}, t_{c2} = chemical kinetics time scales for first order and second order reactions, respectively, defined in Fig. 1, s
u = mean velocity of gas mixture, perpendicular to propellant surface, m/s
W = molecular weight, kg/mol
w_1, w_2 = primary and secondary reaction rates, respectively, mol/m^3-s
Y = mass fraction
y = length coordinate, m
$\alpha_{i,j}$ = reaction rate coefficients in ith reaction, for jth species, defined in text following Eqs. (9) and (10)
δ_f = reactive overall length scale in gaseous flame, m
ϵ = small perturbation quantity, ratio of two length scales, defined in Eq. (1)
ζ = dimensionless near field coordinate in the gas, defined by Eq. (17)
θ = dimensionless enthalpy in liquid phase, $C_c(T-T_m)/Q_{\text{liq}}$
λ = thermal conductivity, J/m-s-K
Λ = flame speed eigenvalue, based on maximal primary reaction rate, defined in Eq. (20)
ρ = mixture density, kg/m^3
$\nu'_{i,j}, \nu''_{i,j}$ = stoichiometric coefficient of jth species in the ith reaction; single and double primes denote reactant and product, respectively
$\phi_j(y)$ = dependent variable in gas phase formulation

Subscripts

c = condensed phase property
eq = equivalent
f = final flame conditions
g = gas phase
H = HMX property
i = primary decomposition ($i=1$) and secondary reaction ($i=2$)
j = chemical species, (for $j=1,2,3...M-1$) and thermal enthalpy, for $j=M$
liq = liquid phase
M = total number of dependent variables in nonlinear gas phase model
m = property corresponding to melting
max = maximal
s = liquid-gas interface
sub = sublimation
0 = 1) ambient (solid phase) temperature, T_0, or 2) low-pressure limit properties m_0, Λ_0

Superscripts

$\tilde{(\ )}$ = dimensionless property
$\bar{(\ )}$ = mean property
$(\ )^*$ = specific (per unit mass): Q_1 is specific heat of reaction, J/kg, and w_1 is reaction rate in kg/m^3-s
$(\ )'$ = abbreviated first derivative, d/dy

Presented as Paper 79-1133 at the AIAA/SAE/ASME 15th Joint Propulsion Conference, June 18-20, 1979; submitted July 31, 1979; revision received March 17, 1981.

*Ph.D. Candidate. Present address: Princeton Combustion Research Labs., Princeton, N.J.

†Senior Professional Staff Member. Present address: AFOSR/NA, Bolling AFB, Washington, D.C. Associate Fellow AIAA.

Introduction

THE deflagration of cyclic nitramine propellants is known to exhibit several unique and complex characteristics, for which a full explanation is still being sought. Since nitramines can deflagrate as monopropellants, a natural and necessary starting point for elucidating the deflagration mechanism is the investigation of neat nitramine combustion. Experimental observations point to complicated decomposition mechanisms (which may proceed in both condensed and vapor phases), extended gaseous reaction region, the formation of a liquid layer, and a variable burning rate pressure exponent. The question is how these elements combine in the overall deflagration process and what their relative influence is upon burning rate. Broader questions concern methods for modifying nitramine burning rate.

Detailed analyses of solid propellant deflagration traditionally incorporate a single overall reaction, with an imposed order (e.g., twice that of the measured burning rate pressure exponent). This type of modeling ensures that the calculated burning rate will exhibit the correct pressure dependence, but often may be at odds with observations of the chemical kinetics of the process, and, for example, cannot explain a variable pressure exponent. A complex flame structure, such as that indicated for nitramines, cannot be expected to be represented adequately by the available single overall reaction models, even in an approximate way. In this instance, a more elaborate modeling effort is necessary to describe nitramine deflagration in particular. Therefore, the present theoretical approach is characterized by the following aspects:

1) It is aimed primarily at testing the combined effects of particular chemical mechanisms, kinetics data and available thermophysical properties, rather than calculating the burning rate.

2) It allows for distinct, simultaneous reactions in the gas phase.

Therefore, the objectives are to reveal the structure of the deflagration wave and the various chemical and physical interactions leading to an observed burning rate pressure dependence, through utilization of available thermochemical and thermophysical data in a detailed combustion model. Evidently, this type of modeling involves a considerable loss of simplicity, compared to the single reaction models; however, it is hoped that the physical insight gained justifies inherent complexities of the model.

The deflagration model herein is applied in the pressure range between 1 and 5 MPa, roughly the lower half of the rocket operating regime. The calculations were performed with available HMX data; comparisons are made with RDX results reported previously.

Physical Considerations

The decomposition kinetics of cyclic nitramines (RDX and HMX) have been investigated extensively over the past thirty years at temperatures both above and below the melting points, mostly at pressures far below those associated with steady deflagration of these substances. Notably, the works of Robertson[1] on the liquid phase and dilute-solution kinetics, Rogers and co-workers[2-4] and Flanigan[5] on condensed and gas phase decomposition, Batten and Murdie[6-9] on the initial condensed phase decomposition stages and their catalysis (proposing an intermolecular mechanism) and Rauch and Fanelli,[10] who identified NO_2 and the effects of secondary reactions in the vapor phase.

Based on unique isotope labeling experiments, Suryanarayana et al.[11] proposed a concerted intramolecular condensed phase decomposition mechanism, initiated by C-N bond fission and leading to the production of equal molar proportions of N_2O and CH_2O. Cosgrove and Owen[12-14] suggested a detailed gas phase mechanism, of which the leading step is N-N bond fission; they have outlined a different reaction path for the condensed phase decomposition, following the oxadiazole-intermediate considered by Robertson[1] as the plausible initial step.

Recently Goshgarian[15] obtained detailed concentration-temperature profiles for RDX and HMX undergoing rapid decomposition through use of mass spectrometry. The presence of NO_2 under both melting and deflagration conditions was indicated, verifying the earlier findings of Rauch and Fanelli[10]; likewise, some of the heavier intermediate fragments considered by Cosgrove and Owen[12-14] (e.g., at 75 and 148 amu) were also detected.

Although most of the kinetic data obtained in these studies is generally in good agreement with the data of Robertson[1] regarding overall primary decomposition, the mechanism indicated is complex and not fully understood. In the case of HMX, the problem is further compounded by the existence of four solid state polymorphs, and the coincidence of exothermic decomposition with melting, effectively interfering with the experimental determination of the fusion enthalpy. However, the following several trends are rather clear. 1) Initial decomposition may occur in both vapor and condensed states, following unimolecular-overall kinetics. 2) The mechanism in the condensed phase is probably initiated by C-N bond fission (in inter- or intra-molecular mode), whereas in the gas phase N-NO_2 bond rupture seems to be the most likely initial step (Shaw and Walker[16] proposed recently HONO elimination as an additional plausible initial step) leading consequently to different decomposition mechanisms for the vapor and condensed states. 3) A large number of secondary reactions may be proposed, leading to final combustion products and flame temperatures. The kinetic time scales associated with some of these reactions as well as primary decomposition are plotted in Fig. 1, showing pronounced diversity. In recent Soviet literature, a fundamental importance is attributed to these secondary reactions regarding heat available for sustaining deflagration. Particularly, reactions leading to (endothermic) NO, as opposed to N_2 formation, considered by Fogelzang et al.[17] and by Kondrikov and Sidorova[18] who correlated burning rate with final flame temperature for a large number of secondary explosives. Elementary secondary reaction steps relevant to nitramines were reviewed recently by McCarty,[19] and a list of relevant kinetic data was compiled by Levy.[20]

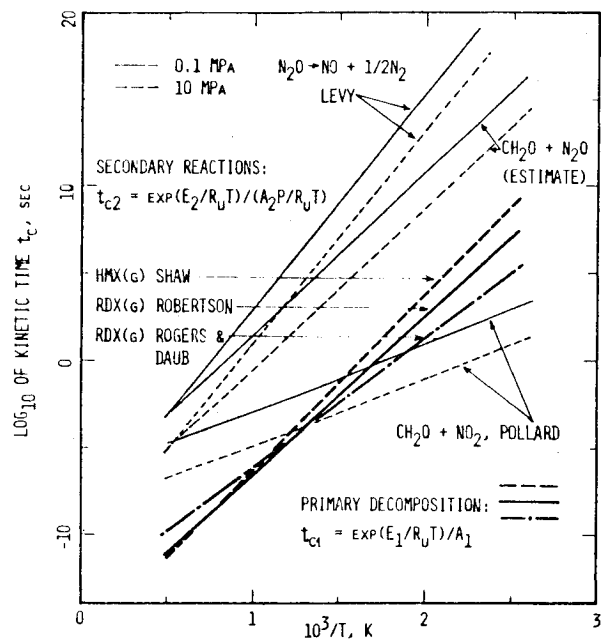

Fig. 1 Comparison of characteristic kinetic times for primary decomposition and secondary reactions in the gas phase plotted against inverse temperature. Clearly primary decomposition is considerably faster except for the $CH_2O + NO_2$ reaction at temperatures below 700 K.

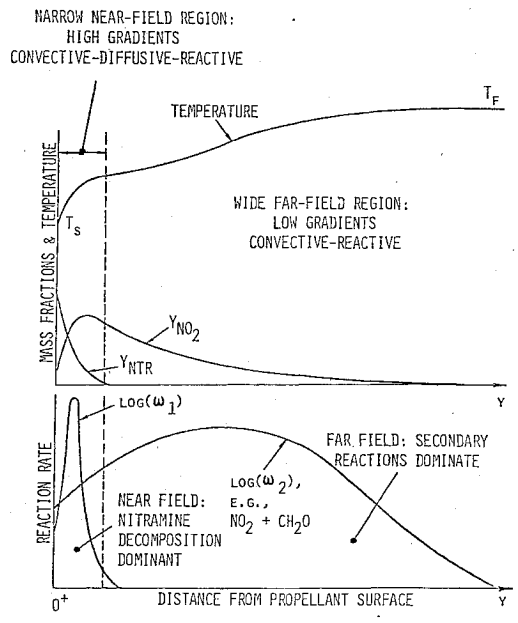

Fig. 2 Gas phase diagram, showing the near-field and far-field configuration for the nitramine deflagration wave (the near-field region is magnified for clarity).

Experimental observations of RDX and HMX combustion indicate that a unique deflagration mechanism might be involved. Burning rate measurements of the pure substances made by Bobolev et al.[21] and by Price and co-workers[22] show that the burning rate pressure exponent tends to increase from roughly 0.5 at low pressures (1 MPa) to 1.0 at high pressures (30 MPa). High-speed shadowgraphs taken in this laboratory[23] demonstrate extended heat release by exothermic reactions in the plume of strand burning samples of HMX (burning at 2.1 MPa), appreciably differing from parallel plume observations made with ammonium perchlorate (AP) where the extent of such heat release seems negligible in comparison. Finally, RDX and HMX in pure granular form or in propellant matrix with inert binder exhibit burning rate pressure exponent breaks[21,24,25] at certain critical high pressures which are granulation size dependent, in a manner completely different from deflagration of AP propellants.

The experimental evidence leads to the conclusion that the nitramine deflagration mechanism differs substantially from that of AP in the pressure range of interest, and a modeling effort aimed specifically at nitramines is therefore warranted.

In the vapor phase, two major reaction categories can be defined. The first is primary decomposition reactions, relatively rapid, unimolecular-overall, forming mainly reactive products (not necessarily heavy fragments) such as CH_2O, NO_2, and N_2O. Second, these products may undergo further reactions, somewhat slower, typically second order overall. These reactions lead finally to complete combustion products such as H_2O, CO, CO_2, N_2, and NO and the observed final flame temperatures. Regarding the actual chemical processes, the foregoing terminology is somewhat artificial since the reactions occur simultaneously for the most part and are thermally and chemically coupled; the main purpose of these definitions is to introduce some modeling idealizations. The comparison of associated kinetic time scales shown in Fig. 1 lends some credibility to the classification considered, demonstrating that at least two overall reactions should be incorporated, owing to the large observed differences in kinetic rates.

The consideration of two overall chemical reactions with distinct length scales has led to the physical picture of the gaseous deflagration region depicted in Fig. 2. The model postulates a high-gradient, relatively thin near field (adjacent to the propellant surface) where primary decomposition dominates and an extended far field (dominated by secondary reactions) where gradients are small in comparison. This has allowed statement of the nitramine deflagration problem in terms of a singular small perturbation theory by Ben-Reuven,[26] the small perturbation quantity being the ratio of two length scales,

$$\epsilon = \frac{\overline{\rho D}/m}{m/\tilde{w}_2} \ll 1 \tag{1}$$

The two overall-reaction configuration leads directly to the following derivation of an asymptotic burning rate equation.[26]

At a given pressure, the equivalent reaction rate is considered

$$w_{eq} \sim w_1 + w_2$$

and its mean value is defined,

$$\tilde{w}_{eq} \sim \tilde{w}_1 + \tilde{w}_2 \quad \text{with} \quad \tilde{w}_1 = F_i(\bar{T}_i)p^i, \quad i=1,2$$

Integrating over the entire gaseous reaction zone, an overall reactive length scale δ_f is defined,

$$\tilde{w}_{eq}\delta_f = \int_0^\infty w_{eq}(y)\,dy \sim m \tag{2}$$

where the last proportionality is implied by the conversion of the entire reactant mixture entering the field at $y=0$ to products of combustion at infinity. The first integral of the energy equation yields

$$m\bar{C}_p\Delta T_f + \frac{\bar{\lambda}\Delta T_f}{\delta_f} \sim Q_{eq}\int_0^\infty w_{eq}\,dy \tag{3}$$

with ΔT_f the net temperature gain throughout the gaseous reaction zone, and $\Delta T_f/\delta_f$ represents the heat feedback gradient at the propellant surface. After using Eq. (2) and some manipulation, the last equation becomes

$$1 + (\bar{\lambda}/m\bar{C}_p)/\delta_f \sim Q_{eq}/\bar{C}_p\Delta T_f \sim 0(1) \tag{4}$$

where the second proportionality arises since the net thermal gain throughout the deflagration wave is due to heat release by reactions. Thus, and since the overall process is expected to be convective-diffusive-reactive, it must also be that

$$(\lambda/m\bar{C}_p)/\delta_f = (\overline{\lambda/C_p})\,\tilde{w}_{eq}/m^2$$
$$= (\overline{\lambda/C_p})\,(\tilde{w}_1 + \tilde{w}_2)/m^2 \sim 0(1) \tag{5}$$

from which the asymptotic burning rate relationship is derived directly,

$$m = ap^{1/2}(1 + p/B_p)^{1/2} \tag{6}$$

where

$$B_p = F_1(\bar{T}_1)/F_2(\bar{T}_2)$$

serves as a reference pressure and a is a proportionality constant. Evidently, at the limit of low pressures, as

$$p \ll B_p, \quad m \sim p^{0.5}$$

whereas at the high pressure limit, as

$$p \gg B_p, \quad m \sim p^1$$

The burning rate data of Bobolev et al.[21] (RDX) and of Price et al.[22] (HMX) are plotted over a wide pressure range in Fig. 3 and correlated by Eq. (6), utilizing a least squares fit for the

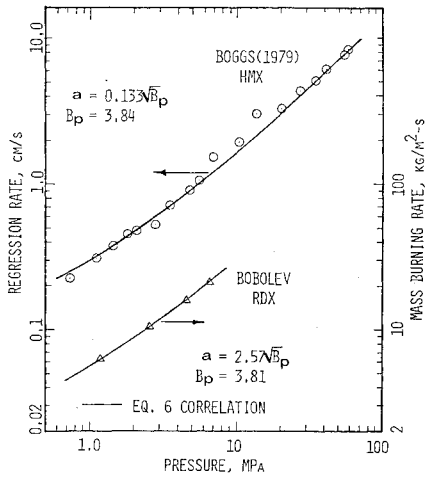

Fig. 3 Experimental burning rate data correlations for the measurements of Price et al. (HMX) and Bobolev (RDX), using Eq. (6), showing that the upward shift of the pressure exponent is followed by the correlation.

linear relationship

$$m^2/p = a^2 + (a^2/B_p)p$$

A good correlation of the data is demonstrated.

To study the processes that influence directly the gas generation at the propellant surface, attention is focused on the near field in the gas. The remainder of the present study is concerned, therefore, with this particular region. It should be stressed that the far field, dominated by secondary reactions, has a nonvanishing effect upon heat feedback to the propellant surface within the pressure range considered (this influence is expected to increase at higher pressures); however, its influence enters only indirectly, through coupling with the near field.

Analytical Model

A nonlinear model for the steady deflagration of nitramine monopropellant has been derived and discussed in detail in Ref. 26; a concise version was presented in the 16th Combustion Symposium (International)[27] in 1976. Presently, the following two overall reactions are considered in the gas phase:

$$\mathrm{HMX(g)} \rightarrow 4/3\mathrm{NO_2} + 4/3\mathrm{N_2O} + 4\mathrm{CH_2O} + 2\mathrm{N_2}$$

$$Q_1 = 134 \text{ kcal} \tag{7a}$$

$$\mathrm{NO_2} + 5/7\mathrm{CH_2O} \rightarrow \mathrm{NO} + 3/7\mathrm{CO} + 2/7\mathrm{CO_2} + 5/7\mathrm{H_2O}$$

$$Q_2 = 46 \text{ kcal} \tag{7b}$$

The overall primary decomposition reaction, Eq. (7a), was obtained from the analogous step for RDX(g), based on the mechanism proposed by Cosgrove and Owen,[12-14] assuming it remains valid for HMX as well. The secondary overall reaction, Eq. (7b), is from Pollard and Wyatt,[28-30] observed to be of first order with respect to each of the reactants. Secondary reactions other than $NO_2 + CH_2O$, as shown in Fig. 1, probably occur in the near field as well, but owing to their relative slowness, are not expected to contribute significantly to the thermal or species balances in this region.

Unfortunately, experimental kinetics data related to primary decomposition of HMX in the vapor phase do not exist, the single result by Rogers and Daub[3,4] notwithstanding. Their kinetic constant matches excellently that obtained by Robertson[1] for HMX decomposition in the liquid phase. Assuming that N-NO_2 fission is the initial rate controlling step in primary decomposition of HMX(g) the calculated results of Shaw and Walker,[16] derived from similarity with dimethylnitramine, were utilized

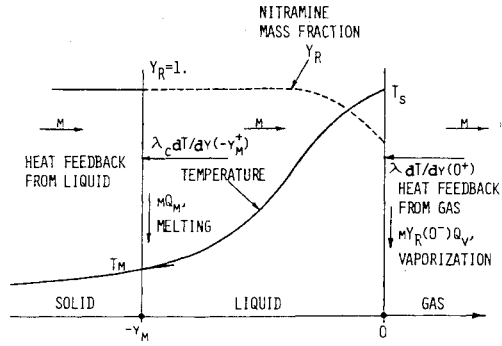

Fig. 4 Diagram of the liquid phase processes for deflagrating nitramine monopropellant at moderate pressures; the rate and extent of decomposition depend upon both local temperature and residence time, with the latter inversely dependent on the flame speed.

$$\log_{10}(k_1) = 16.4 - 46.2/2.3R_uT \tag{8a}$$

and for the $CH_2O + NO_2$ reaction,[28-30]

$$\log_{10}(k_2) = 6.0 - 19/2.3R_uT \text{ for } T > 430\,\mathrm{K} \tag{8b}$$

where k_1 is in 1/s and k_2 in m^3/mol-s.

The gas phase equations of motion in dimensional form, for $0 < y < \infty$

$$m\mathrm{d}\phi_j/\mathrm{d}y - \mathrm{d}(\rho D\mathrm{d}\phi_j/\mathrm{d}y)/\mathrm{d}y = \alpha_{1,j}w_1 + \alpha_{2,j}w_2 \qquad j = 1,2\ldots M \tag{9}$$

The total mass flux is $m = \rho u = \text{const}$, $\phi_j(y)$ represents the mass fractions $Y_j(y)$ for $j = 1,2\ldots M-1$ (in which case $\alpha_{i,j} = W_j(\nu_j'' - \nu_j')_i$, $i = 1, 2$) and thermal enthalpy,

$$\phi_M(y) = h_T = \int_{T_0}^{T(y)} C_p(T)\,\mathrm{d}T \tag{10}$$

for which $\alpha_{i,M} = Q_i$, $i = 1,2$. The reaction rates are

$$w_1 = \rho k_1 Y_H / W_H$$

and

$$w_2 = \rho^2 k_2 (Y_{\mathrm{CH_2O}}/W_{\mathrm{CH_2O}})(Y_{\mathrm{NO_2}}/W_{\mathrm{NO_2}})$$

The nine species involved in Eq. (7) and the enthalpy constitute $M = 10$ unknown variables. After introduction of suitable approximations for the variable specific heat and thermal conductivity, $C_p(Y_1 \ldots Y_{M-1}, T)$ and $\lambda(Y_1 \ldots Y_{M-1}, T)$, detailed in Ref. 26, the near field in the gas is represented by the coupled, nonlinear system of differential equations of the form given by Eq. (9); this amounts to a two-point boundary value problem, with the boundary conditions,

$$\phi_j(0^+) = \phi_j^0 \tag{11a}$$

$$\mathrm{d}\phi_j/\mathrm{d}y(\infty) = 0 \text{ for } j = 1,2\ldots M \tag{11b}$$

Specifying (m, p, T_0) and ϕ_j^0, results in a well-posed problem, for which solutions can be obtained numerically; the finite-difference algorithm was described previously.[27]

The second element in the overall deflagration model is the condensed phase. Following experimental observations of a reacting liquid layer during deflagration of RDX and HMX[15,25,31-34] within the pressure range of interest, the

proposed reacting liquid phase model is shown schematically in Fig. 4. The liquid phase decomposition mechanism proposed is an extension of the initial steps suggested originally by Robertson,[1] and described as follows:

1) HMX(liq) → Oxadiazole intermediate → (four-center process)

2) CH_2O + [large fragment → $N_2O + 3CH_2=N-NO_2$]

3) $CH_2=N-NO_2 \rightarrow CH_2O + N_2O$

A possible route for the last depolymerization step was suggested by Suryanarayana[11]; as mentioned earlier, heavy fragments of 148 and 75 amu were detected in deflagrating HMX,[15] the latter possibly arising from rapid proton absorption by $CH_2=N-NO_2$. Assuming additionally a limited degree of secondary reaction,

4) $N_2O \rightarrow NO + \frac{1}{2}N_2$ (for one mole only)

which is slightly endothermic, the overall reaction step can be summarized

$$HMX(liq) \rightarrow 4CH_2O + 3N_2O + NO + \tfrac{1}{2}N_2$$

$$Q_{liq} = 60 \text{ kcal/mol} \tag{12a}$$

with the unimolecular-overall kinetic constant,[1]

$$\log_{10}(k_{liq}) = 19.7 - 52.7/2.3R_uT \tag{12b}$$

The physical process can be described as follows. Beta-HMX, the polymorph stable at room temperature, is heated up from ambient temperature T_0. Due to the rapid heating typical to deflagration, transition to delta-HMX (occurring under slow heating rates at 471 K) is assumed to be deferred to the melting point, at 554 K. According to Hall,[35] the heat of transition is −2.35 kcal/mol (endothermic); experimental values for the fusion enthalpy Q_m do not exist. However, Rosen and Dickinson[36] noted that the specific (per unit mass) sublimation enthalpies of RDX and HMX are almost equal so that the molar values are related as follows:

$$Q_{sub}(\text{RDX})/3 \doteq Q_{sub}(\text{beta-HMX})/4 \doteq 10.4 \text{ kcal/mol}$$

which can be largely attributed to intermolecular interaction, due to the close proximity of C---O between neighboring molecules in the crystal; the contribution of this bond to nitramine crystal stability was pointed out by Belyayeva et al.[37] By analogy, the fusion enthalpies may be similarly related, resulting in the following estimate for HMX: $Q_m(\text{beta-HMX}) \doteq 4/3$ $Q_m(\text{RDX}) = 11.4$ kcal/mol, where $Q_m(\text{RDX}) = 8.52$ kcal/mol according to Hall.[35]

Following melting, the exothermic decomposition reaction may proceed according to the local temperature and HMX concentration in a first-order manner, assuming gaseous products to be dissolved in the liquid. This process continues through the duration of the melt layer, until gasification occurs at the $y = 0$ interface, where the heat of evaporation Q_v is depleted. The two equations of motion involve temperature and nitramine species; in dimensional form they are

$$\lambda_c d^2T/dy^2 - mC_c dT/dy = -\rho_c Y_H k_{liq}(T) Q_{liq} \tag{13a}$$

$$m dY_H/dy = -\rho_c Y_H k_{liq}(T) \tag{13b}$$

for $-y_m < y < 0$, assuming negligible molecular diffusion and uniform thermophysical properties. The remainder of the liquid phase species mass fractions can be obtained from Y_H through suitable Shvab-Zeldovich coupling terms. The melt thickness y_m is unknown, and an auxiliary relationship is required; this is given by the energy balance at the solid-liquid interface,

$$\lambda_c dT/dy_c(0^+) = Q_m + C_c(T_m - T_0) \tag{14}$$

with the coordinate transform $y_c = y + y_m$. The conditions at $y_c = 0^+$ are specified as follows:

$$T(0^+) = T_m, \quad Y_H(0^+) = 1 \tag{15}$$

Further transform[26] of Eqs. (13-15) leads to an equivalent initial value problem, with dimensionless temperature as the independent variable, which can be integrated forward from $T = T_m$ until a specified T_s is reached.[26]

Evidently, gas phase and condensed phase integrations can be carried out separately by specifying boundary data at the liquid-gas interface,

$$Y_1(0^+), \ldots Y_{M-1}(0^+), \; T_s$$

the values of which are unknown a priori. To render the system physically meaningful, the species and enthalpy conservation conditions across the liquid-gas interface must be satisfied; in dimensionless form, following Scala and Sutton,[38]

$$Y_j(0^+) - dY_j/d\zeta(0^+) = Y_j(0^-), \quad j = 1,2 \ldots M-1 \tag{16a}$$

$$\tilde{h}(0^+) - d\tilde{h}/d\zeta(0^+) = \tilde{h}_c(0^-) - q_c \tag{16b}$$

$$q_c = [\lambda_c dT/dy(0^-) + mY_H(0^-)Q_v]/mQ_1^* \tag{16c}$$

where $\tilde{h} = h_T/Q_1^*$, $\tilde{h}_c(0^-) = C_cT_s/Q_1^*$ and the near field dimensionless coordinate is defined

$$\zeta = \int_0^y \frac{dy}{(\rho D/m)} \tag{17}$$

Solution manifolds can be generated now for specified (m, p, T_0) data. The actual surface procedure involves finite-difference approximation of the derivatives in Eqs. (16a) and (16b), using a three-point, second-order accurate formula; the $\phi_j(0^+)$ vector, therefore, can be calculated and then used to obtain the solution of the liquid and gas fields in an iterative time-like relaxation. The solution is termed converged when the variation of the vector ϕ_j over the entire domain in $y \geq 0^+$, within a single iteration, is smaller than a predetermined value; this value is such that all of the conditions in Eqs. (16a) and (16b) are satisfied within an error of 0.5% in absolute magnitude. Regarding the treatment of the interface conditions and the manner by which gas and liquid phase solutions are combined in the overall solution procedure, the present treatment (following Ref. 26) differs from that of Ref. 27.

Discussion of Results

As mentioned earlier, the present mode of solution by the nonlinear algorithm requires the burning rate $m(p, T_0)$ as input, rather than solve for it. Solutions which include m as output are entirely possible and the method for obtaining them was tested previously (for RDX).

The burning rate correlation, Eq. (6), for Price's HMX data[22] was utilized for imposing $m(p; T_0 = 298 \text{ K})$ in the nonlinear algorithm. Thermophysical and thermochemical properties used as input for generation of the HMX solutions discussed herein are summarized in Ref. 26.

The near field structure is revealed in Figs. 5a-c where temperature, mass fractions (of primary decomposition species), and reaction rates w_1 and w_2 are plotted against distance from the propellant surface. Three distinct $(m; p)$ values serve as parameters in each of these diagrams. Dimensional gradients $d\phi_j/dy$ as well as w_1 and w_2 are shown to increase as pressure is increased. The secondary reaction w_2, unlike w_1, does not peak within the near field. The near-field thickness, as indicated by the distance for complete nitramine depletion in Fig. 5b decreases with pressure, whereas the corresponding final temperature (approximately

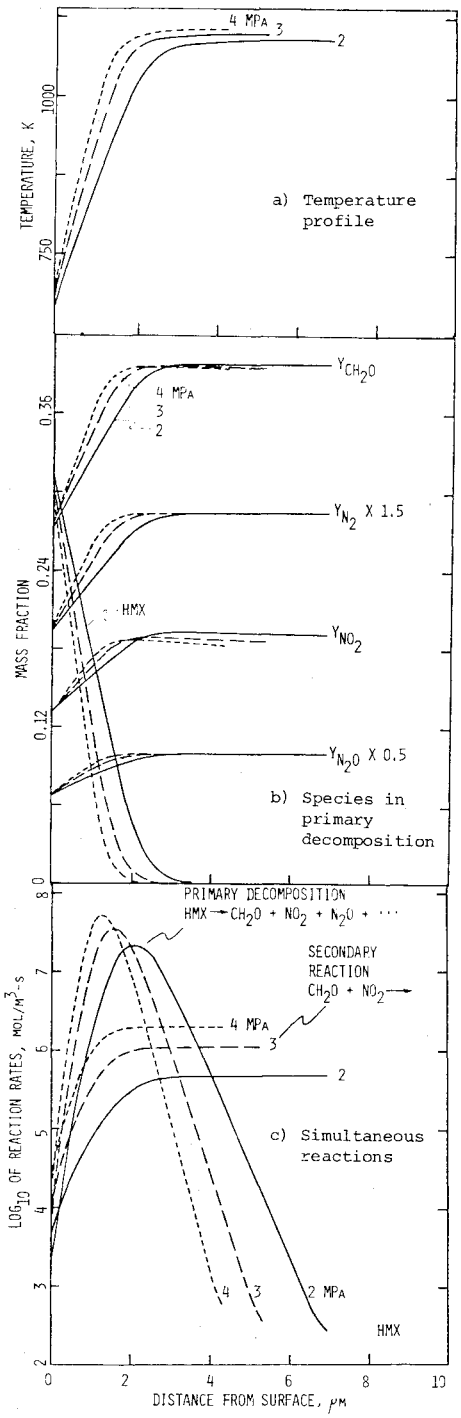

Fig. 5 Near-field distribution for HMX deflagration at three pressures.

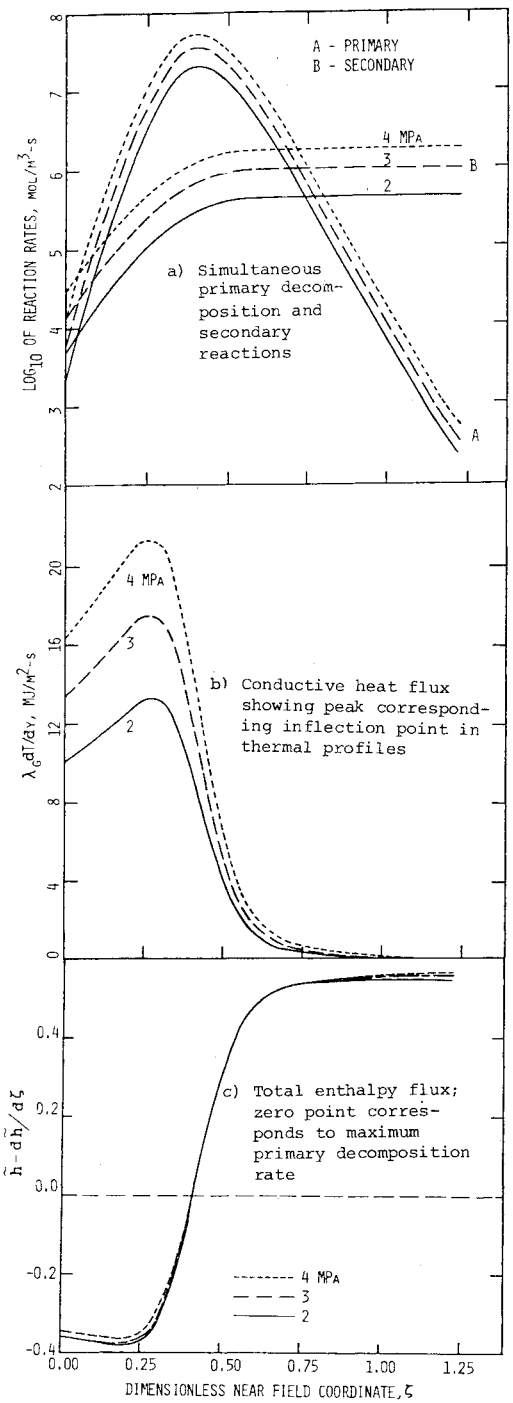

Fig. 6 Near-field distribution for HMX deflagration expressed in terms of dimensionless space coordinate.

a third of the final flame temperature T_f) is shown to increase. The secondary reaction products CO, CO_2, H_2O, and NO (not shown) have mass fractions typically one to two orders of magnitude lower than the primary reaction species and increase continuously throughout the near field. Several near field properties are drawn as a function of the dimensionless near field coordinate ζ, defined by Eq. (17), in Figs. 6a-c. The reaction rate plot in Fig. 6a shows that peaking of the primary reaction rate occurs at a unique near field position, $\zeta \doteq 0.4$, apparently regardless of pressure, which is of physical significance and will be discussed later. Note also that $w_2 > w_1$ at $\zeta = 0^+$, due to the lower activation energy of w_2. In Fig. 6b the conductive heat feedback profiles are drawn, showing significant overall increase with pressure within the near field. This function has a maximum, somewhat off the surface; again the locus of maxima appears invariant to pressure. The total dimensionless enthalpy flux, $h - \mathrm{d}h/\mathrm{d}\zeta$, is plotted in Fig. 6c. The curves for distinct pressures lie very close, indicating near self-similar behavior. The negative portion, for $0^+ < \zeta < 0.4$ shows net thermal transport toward the propellant surface, while the positive portion ($\zeta > 0.4$) indicates net outward transport of enthalpy. The point where this function is zero (and undergoes maximal variation) coincides with $w_{1,\max}$ where chemical heat release is maximal; the point therefore can be considered as a continental divide within the near field, regarding thermal transport.

In the process of obtaining numerical solutions at various pressures, all input parameters are normally fixed while various (m, p) are imposed. Following several unsuccessful attempts to obtain convergence for $p < 4$ MPa, it became

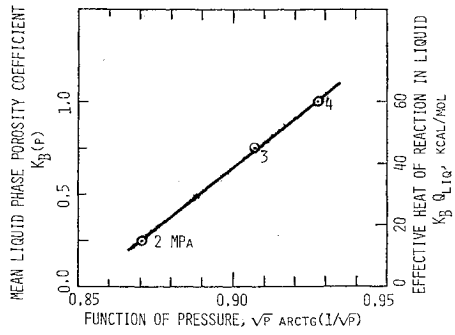

Fig. 7 Mean liquid phase porosity coefficient $K_B(p)$, due to subsurface decomposition yielding gaseous products, and the resultant effective heat of reaction in the liquid $K_B Q_{liq}$, correlated with the pressure dependence of the mean melt layer density.

evident that solutions could not be generated at these pressures unless Q_{liq} was decreased to values appreciably below that given in Eq. (12a). Additional solutions were then generated at 2 and 3 MPa by trial and error. The systematic variation of $K_B(p)Q_{liq}$, where K_B (as yet unspecified) contains the pressure variation, was then investigated. Attempts to correlate with p, p^2, or logarithmic correlations vs $1/T_s$, as well as combinations thereof, all failed. Thus, the possibility of thermal cause, either by first order, second order or heterogeneous reactions were considered unlikely. However, as shown in Eq. (13a), the liquid phase density multiplies the reaction rate term. If bubbles were formed (due to gaseous products of liquid phase decomposition) their presence could modify the density of the melt layer appreciably and introduce pressure dependence. Denoting the local aggregate density by ρ_c^* and assuming that 1) bubbles are small and hence their inner properties are uniform, and are at thermal equilibrium with surrounding liquid; 2) bubbles are convected with the local mean aggregate velocity, i.e., no bubble diffusion; and 3) pressure throughout the layer is uniform, and bouyancy forces negligible; it can be shown that

$$\rho_c^*/\rho_H = 1/[Y_H + (1-Y_H)\rho_H/\rho_g] \tag{18}$$

where ρ_H is the pure liquid density,

$$\rho_g = p\bar{W}_g/R_u T(y)$$

is the bubble gas density, and $Y_H(y)$ is now the local nitramine mass fraction, defined over the aggregate (the liquid being pure nitramine). The preceding compressibility ratio is, of course, variable with $Y_H(y)$ and $T(y)$. To elucidate its mean pressure dependence, some approximations are introduced. Assuming that $Y_H \sim 1 - a\theta^2$ where

$$0 \le \theta = (T - T_m)/(Q_{liq}/C_c) < 1$$

is the dimensionless temperature, substitution of Y_H and T according to these expressions in Eq. (18) and neglecting the resulting θ^3 term leads to

$$K_B(p) = \bar{\rho}_c/\rho_H \sim \frac{1}{\theta_s}\int_0^{\theta_s} \frac{d\theta}{(1+C^2\theta^2)} \sim \arctan(C)/C \tag{19}$$

where $C^2 \sim 1/p$ and $\theta_s = \theta(T_s)$. Therefore, $K_B(p) \sim p^{0.5} \arctan(p^{-0.5})$. Indeed, this functional pressure dependence was found to correlate the variable $K_B Q_{liq}$ excellently, as shown in Fig. 7. The presence of bubbles in the reacting liquid layer of deflagrating HMX within the pressure range tested is therefore strongly inferred, in agreement with experimental observations.[34]

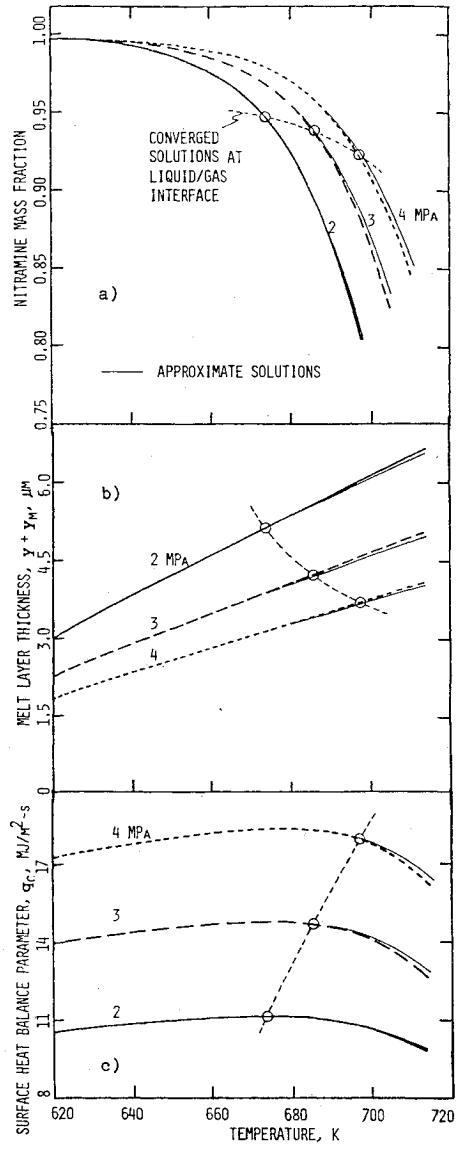

Fig. 8 Melt layer profiles vs temperature for three distinct data sets (m, p, $K_B Q_{liq}$).

Liquid layer profiles, corresponding to solutions at three distinct (m, p, Q_{liq}) data sets are shown in Figs. 8a-c, plotted against temperature. The HMX mass fraction in Fig. 8a is shown to decrease with increasing T in the layer, in a manner suggesting the approximation $Y_H \sim 1 - a\theta^2$ mentioned earlier. The total amount depleted is a function of residence time, $\sim 1/m^2$ and mean layer temperature $\sim T_s$. These effects counteract, since m and T_s increase with p; the thermal effect is shown stronger, as expected, such that $Y_H(0^-)$ is decreasing with pressure for converged solutions. The liquid layer coordinate, $y+y_m$, is depicted in Fig. 8b, showing the variation of temperature with distance; the layer thickness decreases with increasing pressure. The surface heat balance parameter $mQ_f^* q_c$ defined by Eq. (16c) is plotted in Fig. 8c. Peaking of this function is due to peaking of $\lambda_c dT/dy_c$ in the layer, caused by the exothermic reaction. When heat release is negligible (low T), $\lambda dT/dy_c \sim T$; however, as temperature increases the heat release by decomposition increases, and progressively less heat feedback is required to maintain any particular temperature. Accompanying each of the liquid phase curves in Fig. 8 is a thin line, representing an approximate analytical solution[26] where all heat release due to

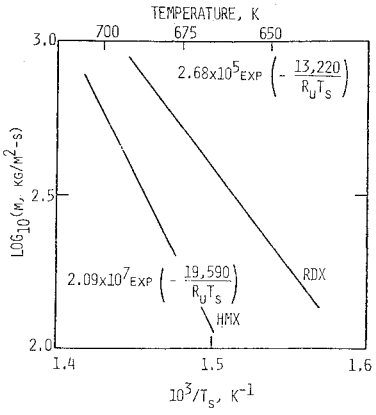

Fig. 9 Burning rate vs calculated inverse surface temperature. Arrhenius-type correlations demonstrated for both HMX and RDX with HMX shown to have somewhat higher apparent activation energy.

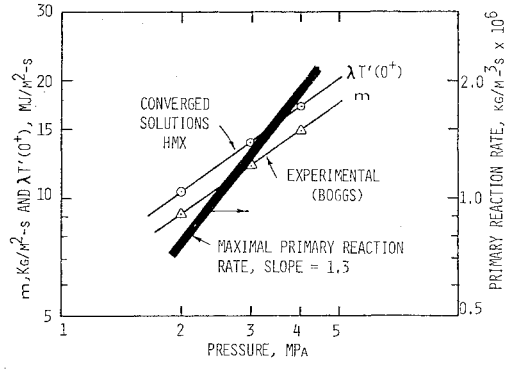

Fig. 10 Mass burning rate and conductive heat feedback from the gas to the propellant surface showing that the correlations have similar pressure exponents. The pressure exponent of the maximal primary reaction rate demonstrating thermal enhancement due to secondary reaction.

decomposition is deferred to the surface. These clearly obtain good approximations except for the thermal gradient (not shown) where they are linear in T.

Similar liquid phase profiles for RDX were shown in Ref. 27; these results were erroneously generated for an endothermic decomposition. Fortunately, due to the relatively small extent of decomposition, the trends of the converged results were not affected substantially. The correct form[26] is similar to the results shown in Fig. 8.

To assess the effect of condensed phase exothermicity upon burning rate, the following criterion has been proposed,[26]

$$g_c = [\lambda_g T'(0^+)_{NR} - \lambda_g T'(0^+)_{RC}]/\lambda_g T'(0^+)_{RC}$$

where subscripts NR and RC denote nonreacting and reacting condensed phase, respectively, both heat feedback terms calculated at the same values of $(m;\ T_s)$. The values of g_c obtained for HMX are 9.7, 10.7, and 13.8% at 2, 3, and 4 MPa, respectively, increasing in an accelerated manner. For RDX, the same trend is followed but at somewhat lower values, between 2 and 8% within 1-4 MPa. Despite the tendency indicated (thinner layer and higher extent of reaction as p increases), further analysis shows[26] that g_c undergoes a maximum at higher pressure, outside of the range considered at present; for RDX this is predicted to occur at 25% of subsurface decomposition. Therefore, the effect is expected to delay somewhat the onset of burning rate control by secondary reactions ($n=1$).

Turning now to properties that demonstrate the overall pressure dependent behavior, Fig. 9 depicts $\log(m)$, the imposed burning rate, against inverse surface temperature obtained from converged solutions. Somewhat surprisingly, a very good Arrhenius-type correlation is observed. This indicates the plausibility of an evaporation law, although the apparent activation energy is somewhat different than the

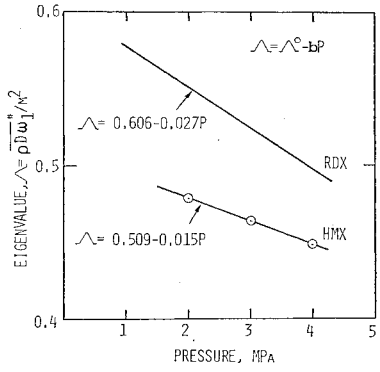

Fig. 11 Flame speed eigenvalue vs pressure showing the linear relationship predicted by the asymptotic flame field theory. (Λ_0 = const is due to zeroth order primary reaction effect, while the small decrement $-bP$, is the first-order contribution by the secondary reaction.)

estimated latent heat of evaporation[36,39] Q_v. The surface temperature is observed to vary between 670 and 700 K for $2 \le P \le 4$ MPa. Values corresponding to RDX[26] are shown for comparison. The burning rate and the heat feedback gradient at the gas side of the $y=0$ interface are plotted vs pressure in Fig. 10; the lines are parallel, indicating that the propellant regression rate is driven by the gas phase in most part. Compared with Fig. 3, the apparent linearity of m in Fig. 10 is merely due to the relatively narrow pressure range herein.

Overplotted in Fig. 10 is the maximal primary reaction rate (cf. Fig. 6a at $\zeta=0.4$). A uniform pressure dependence is demonstrated, but the slope is larger than unity. This enhanced pressure dependence could be explained as thermal catalysis,[26] due to the presence of the secondary reaction in the near field and is extremely important for understanding the mechanism of coupling between secondary reactions and the burning rate. Since heat release by primary decomposition exceeds by far that due to secondary reaction in the near field, the former process can be safely assumed to govern the heat feedback to the surface, as evident from the correspondence between $w_{1,\max}$ and thermal transport, shown in Figs. 6a and 6c. However, the primary reaction rate (due to its large activation energy) is highly sensitive to thermal variation, and would be appreciably amplified by the relatively small secondary reaction heat release. Therefore, it is inferred that the major effect of the secondary reaction upon heat feedback to the surface is through the indirect thermal enhancement of primary decomposition. This effect is roughly ten-fold larger than the ratio of secondary/primary heat release in the near field.

Finally, a plot of the flame speed eigenvalue as function of pressure is given in Fig. 11. The eigenvalue is defined

$$\Lambda = \overline{\rho D w_1^*}/m^2 \tag{20}$$

and $\dot{w}_1^*$ was taken at the maximum of w_1, cf. Fig. 6a. Considering for the moment low pressures, $\dot{w}_1 \sim p$ and m^2 can be expressed by the asymptotic burning rate correlation, Eq. (6)

$$m^2 = a^2 p(1 + p/B_p) = m_0^2(1 + p/B_p) \tag{21}$$

where m_0 is the burning rate at the low pressure limit. After substitution of the m^2 expression in Eq. (20), one obtains

$$\Lambda = \Lambda_0/(1 + p/B_p) \doteq \Lambda_0(1 - p/B_p) \tag{22}$$

where $\Lambda_0 = \overline{\rho D w_1^*}/m_0^2$ and $m_0 = ap^{0.5}$. Λ_0 therefore is independent of pressure, but the actual Λ involves a small decrement, clearly due to secondary reaction effects. This behavior continues into the pressure regime tested, and explains the linear relationship observed for $\Lambda(p)$ in Fig. 11; similar behavior is shown for RDX.

Conclusions

The deflagration wave structures of RDX and HMX have been demonstrated in the 2-5 MPa pressure regime, along

with several pressure dependent characteristics. These may be summarized as follows.

1) The burning rate pressure dependence (variable n) predicted by the asymptotic burning rate formula, Eq. (6), is in good agreement with experimental observations, despite its simplicity. This demonstrates that simultaneous reactions (as opposed to a single overall step) in the flame zone are essential for proper modeling of nitramine deflagration.

2) The primary decomposition reaction rate is thermally enhanced by the presence of the considerably weaker secondary reaction. This points to a mechanism of indirect coupling between the far field processes (secondary reactions) and the burning rate, through which the far field effect is amplified. In this respect the near field region with its dominant primary decomposition has fundamental importance in controlling heat feedback to the propellant surface. Thus, it is anticipated that as pressure increases, a relatively small change in final flame temperature would correspond to an appreciable change in burning rate, as indicated by the correlations of t_f and p made in Refs. 17 and 19.

3) Within the range tested, the linear variation of the flame speed eigenvalue with pressure is explained by the presence of the secondary reaction in the near field. The deviation of Λ from $\Lambda_0 = \text{const}$ is therefore a measure for the influence of the secondary reaction upon the burning rate, both quantitatively and in terms of the pressure dependence.

4) The surface temperature calculated varies with pressure and correlates with the imposed burning rate to yield an Arrhenius-type relationship.

These observations contribute toward a better understanding of the deflagration of nitramines. For future study, the following suggestions are made.

1) The indication of presence of bubbles in the melt layer, discussed in the foregoing section, warrants further investigation by suitable modeling.

2) Solutions which include calculation of burning rates must await the attainment of suitable high temperature evaporation data.

3) More complete modeling of secondary reactions would allow extension of the model over the entire flame zone (to include the far field), as well as to higher pressures.

Acknowledgments

The development of the basic model and initial calculations for RDX were funded by the Power Branch of the Office of Naval Research with supplements provided by the Army Ballistic Research Laboratory. Improvements to the computational procedures and investigation of HMX combustion were funded by the Air Force Rocket Propulsion Laboratory as part of a cooperative effort with Huntsville Division of the Thiokol Corporation.

References

[1] Robertson, A.J.B., "The Thermal Decomposition of Explosives, Part II. Cyclotrimethylenetrinitramine and Cyclotetramethylenetetranitramine," *Transactions of the Faraday Society*, No. 45, 1949, pp. 85-93.

[2] Rogers, R. N., "Differential Scanning Calorimetric Determination of Kinetic Constants of Systems that Melt with Decomposition," *Thermochimica Acta*, No. 3, 1972, pp. 437-447.

[3] Rogers, R. N. and Daub, G. W., "Scanning Calorimetric Determination of Vapor-phase Kinetic Data," *Analytical Chemistry*, Vol. 45, March 1973, pp. 569-570.

[4] Rogers, R. N., "Determination of Condensed Phase Kinetic Constants," *Thermochimica Acta*, No. 9, 1974, pp. 444-446.

[5] Flanigan, D., personal communication, 1979.

[6] Batten, J. J. and Murdie, D. C., "The Thermal Decomposition of RDX at Temperatures Below the Melting Point. Part I: Comments on the Mechanism," *Australian Journal of Chemistry*, Vol. 23, 1970, pp. 737-747.

[7] Batten, J. J. and Murdie, D. C., "The Thermal Decomposition of RDX at Temperatures Below the Melting Point. Part II: Activation Energy," *Australian Journal of Chemistry*, Vol. 23, 1970, pp. 749-755.

[8] Batten, J. J., "The Thermal Decomposition of RDX at Temperatures Below the Melting Point. Part III: Toward Elucidation of the Mechanism," *Australian Journal of Chemistry*, Vol. 24, 1971, pp. 945-954.

[9] Batten, J. J., "The Thermal Decomposition of RDX at Temperatures Below the Melting Point. Part IV: Catalysis of the Decomposition by Formaldehyde," *Australian Journal of Chemistry*, Vol. 24, 1971, pp. 2025-2029.

[10] Rauch, F. C. and Fanelli, A. J., "The Thermal Decomposition Kinetics of Hexahydro, 1, 3, 5-trinitro-s-triazine Above the Melting Point: Evidence for Both a Gas and Liquid Phase Decomposition," *The Journal of Physical Chemistry*, Vol. 73, May 1969, pp. 1604-1608.

[11] Suryanarayana, B., Graybush, R. J., and Autera, J. R., "Thermal Degradation of Secondary Nitramines: A Nitrogen-15 Tracer Study of HMX (1, 3, 5, 7 Tetranitro-1, 3, 5, 7-Tetraazacyclooctane)," *Chemistry and Industry*, Dec. 1967, pp. 2177-2178.

[12] Cosgrove, J. D. and Owen, A. J., "The Thermal Decomposition of 2, 3, 5 Trinitrohexahydro-1, 3, 5 triazine (RDX)," *Chemical Communications*, 1968, p. 286.

[13] Cosgrove, J. D. and Owen, A. J., "The Thermal Decomposition of 1, 3, 5 Trinitro Hexahydro 1, 3, 5 triazine (RDX) Part I: The Products and Physical Parameters," *Combustion and Flame*, No. 22, 1974, pp. 13-18.

[14] Cosgrove, J. D. and Owen, A. J., "The Thermal Decomposition of 1, 3, 5 Trinitro Hexahydro 1, 3, 5 triazine (RDX) Part II: The Effects of the Products," *Combustion and Flame*, No. 22, 1974, pp. 19-22.

[15] Goshgarian, B. B., "The Decomposition of Cyclotrimethylenetrinitramine (RDX) and Cyclotetramethylenetetranitramine," AFRPL-TR-78-76, Oct. 1978.

[16] Shaw, R. and Walker, F. E., "Estimated Kinetics and Thermochemistry of Some Initial Unimolecular Reactions in the Thermal Decomposition of 1, 3, 5, 7 Tetranitro-1, 3, 5, 7 tetraazacyclooctane in the Gas Phase," *The Journal of Physical Chemistry*, Vol. 31, No. 25, 1977, pp. 2572-2576.

[17] Fogelzang, A. E., Svetlov, B. S., Azhemian, V. Ya, Kolyasov, S. M., and Sergienko, O. I., "The Combustion of Nitramines and Nitosamines," translated from *Docladi Academi Nauk*, SSSR, Vol. 216, No. 3, May 1974, pp. 603-606.

[18] Kondrikov, B. N. and Sidorova, T. T., *Docladi Academi Nauk*, SSSR, Vol. 197, No. 7, 1971, pp. 125-128.

[19] McCarty, K. P., "HMX Propellant Combustion Studies: Phase 1, Literature Search and Data Assessment," AFRPL-TR-76-59, Dec. 1976.

[20] Levy, J. B., "Examination of Chemical Kinetics Data used in Induction Zone Calculations for the Combustion of Cordite," BRL CR-310, Aug. 1976.

[21] Bobolev, V. K., Margolin, A. M., and Chuiko, S. V., "Stability of Normal Burning of Porous Systems at Constant Pressure," *Journal of Combustion, Explosion and Shock Waves*, Vol. 2, No. 4, 1966, pp. 15-20.

[22] Price, C. F., Boggs, T. L., and Derr, R. L., "The Steady State Combustion Behavior of Ammonium Perchlorate and HMX," AIAA Paper 79-0164, AIAA 17th Aerospace Sciences Meeting, Jan. 1979.

[23] Caveny, L. H., unpublished high speed film sequences, Princeton University, Princeton, N.J., 1974.

[24] Taylor, J. W., "The Burning of Secondary Explosive Powders by a Convective Mechanism," *Transactions of the Faraday Society*, Vol. 58, No. 471, 1962, pp. 561-568.

[25] Cohen, N. S. and Strand, L. D., "Nitramine Propellant Research," NASA TM 33-801, Oct. 1976.

[26] Ben-Reuven, M. and Caveny, L. H., "Nitramine Monopropellant Deflagration and Nonsteady, Reacting Rocket Chamber Flows," (AD-A085650) MAE Rept. 1455, Jan. 1980, Princeton University, Princeton, N.J.

[27] Ben-Reuven, M., Caveny, L. H., Vichnevetsky, R., and Summerfield, M., "Flame Zone and Subsurface Reaction Model for Deflagrating RDX," *Proceedings of the 16th Symposium (International) on Combustion*, The Combustion Institute, Pittsburgh, Pa., 1976, pp. 1223-1233.

[28] Pollard, F. H. and Wyatt, R.M.H., "Reactions Between Formaldehyde and Nitrogen Dioxide Part I. The Kinetics of the Slow Reaction," *Transactions of the Faraday Society*, Vol. 45, 1949, pp. 760-767.

[29] Pollard, F. H. and Woodward, R., "Reactions Between Formaldehyde and Nitrogen Dioxide. Part II: The Explosive Reaction," *Transactions of the Faraday Society*, Vol. 45, 1949, pp. 767-770.

[30] Pollard, F. H. and Wyatt, R.M.H., "Reactions Between Formaldehyde and Nitrogen Dioxide. Part III: The Determination of Flame Speeds," *Transactions of the Faraday Society*, Vol. 45, 1950, pp. 281-289.

[31] Taylor, J. W., "A Melting Stage in the Burning of Solid Secondary Explosives," *Combustion and Flame*, Vol. 6, June 1962, pp. 103-107.

[32] Cohen, N. S. and Strand, L. D., "Nitramine Propellant Research," *13th JANNAF Combustion Meeting*, CPIA Pub. 281, Vol. 1, 1976, pp. 75-87.

[33] Boggs, T. L., Price, C. F., Zurn, D. E., Derr, R. L., and Dibble, E. J., "The Self-Deflagration of Cyclotetramethylenetetranitramine (HMX)," Paper 77-859, AIAA/SAE 13th Propulsion Conference, Orlando, Fla., July 1977.

[34] Derr, R. L., Boggs, T. L., Zurn, D. E., and Dibble, E. J., "The Combustion Characteristics of HMX," *11th JANNAF Combustion Meeting*, CPIA Pub. 261, Vol. 1, Dec. 1974, pp. 231-241.

[35] Hall, P. G., "Thermal Decomposition and Phase Transitions in Solid Nitramines," *Transactions of the Faraday Society*, Vol. 67, Pt. 2, 1971, pp. 556-562.

[36] Rosen, J. M. and Dickinson, C., "Vapor Pressures and Heats of Sublimation of Some High Melting Organic Explosives," *Journal of Chemical and Engineering Data*, Vol. 14, No. 1, Jan. 1969, pp. 120-124.

[37] Belyayeva, M. S., Klinenko, G. K., Dabaytseva, L. T., and Stolyarov, P. M., "Factors Determining the Thermal Stability of Cyclic Nitroamines in Crystalline State," Moscow, work in translation, 1978.

[38] Scala, S. M. and Sutton, G. W., "Energy Transfer at a Chemically Reacting or Slip Interface," *ARS Journal*, Feb. 1959, pp. 141-143.

[39] Taylor, J. W. and Crookes, R. J., "Vapour Pressure and Enthalpy of Sublimation of 1, 3, 5, 7 Tetranitro-1, 3, 5, 7-tetra-azacyclo-octane (HMX)," *Journal of the Chemical Society*, Faraday Transactions I, Vol. 3, 1976, pp. 723-729.